nature protocols

PROTOCOL

https://doi.org/10.1038/s41596-021-00602-5

Check for updates

Cargo loading within ferritin nanocages in preparation for tumor-targeted delivery

Jianlin Zhang[1,4], Dengfeng Cheng[2,4], Jiuyang He[3,4], Juanji Hong[1], Chang Yuan[1] and Minmin Liang[1]✉

Ferritins are spherical iron storage proteins within cells, composed of 24 subunits of two types, heavy-chain ferritin (HFn) and light-chain ferritin. Ferritins auto-assemble naturally into hollow nanocages with an outer diameter of 12 nm and an interior cavity 8 nm in diameter. Since the intrinsic tumor-targeting property of human HFn was first reported in 2012, HFn has been extensively explored for tumor-targeted delivery of anticancer drugs and diagnostic molecules, including radioisotopes and fluorophores, as well as inorganic nanoparticles (NPs) and chemotherapeutic drugs. This protocol provides four detailed procedures describing how to load four types of cargoes within HFn nanocages that are capable of accurately controlling cargo loading: synthesis of inorganic metal nanoparticles within the cavity of a wild-type human HFn nanocage (Procedure 1, requires ~5 h); loading of doxorubicin into the cavity of a wild-type human HFn nanocage (Procedure 2, requires ~3 d); loading Gd^{3+} into the cavity of a genetically engineered human HFn nanocage (Procedure 3, requires ~20 h); and loading $^{64}Cu^{2+}$ radioisotope into the cavity of a genetically engineered human HFn nanocage (Procedure 4, requires ~3 h). Subsequent use of these HFn-based formulations is advantageous as they have intrinsic tumor-targeting capability and lack immunogenicity. Human HFn generated as described in this protocol can therefore be used to deliver therapeutic drugs and diagnostic signals as multifunctional nanomedicines.

Introduction

Although a variety of types of nanomedicines have been developed for clinical research, to date, only very few have moved into clinical trials[1–4]. This has partially been due to safety concerns, which include a lack of data evaluating the long-term behavior of nanomedicines in vivo[5–8]. Nanocarriers with excellent safety profiles that are capable of specifically binding to a disease state, and simultaneously carrying high doses of diagnostic or therapeutic cargo, are hence much sought after for nanomedical engineering. Human ferritins are spherical iron storage proteins within cells that are composed of a combination of 24 subunits of the heavy-chain ferritin (HFn) and light-chain ferritin[9,10]. Human HFn was reported to have intrinsic tumor-targeting properties[11,12]. As ferritins self-assemble into a nanocages, they have recently been investigated as potential nanocarriers[13–17].

In this protocol, we provide detailed instructions for precise and controlled encapsulation of cargo within human HFn vehicles. To date, more than 50 types of cargo molecules, including drugs, contrast agents, genes and metal NPs, have been loaded into the cavity of ferritin nanocages for a wide range of applications, from biological detection assays to disease diagnosis and biomedicine development. These representative applications are highlighted in Table 1, and include our own use of the protocol we describe here to synthesize iron oxide NPs within the hollow human HFn nanocages[11,18,19] and load doxorubicin into the cavity of human HFn nanocages[17].

Comparison with alternative approaches

In comparison with conventional engineered nanocarriers, the natural human HFn nanocage has the following distinct features that make it suitable for use as a carrier for anticancer therapeutics:

- Intrinsic tumor targeting capability. Without any further modification, human HFn can selectively deliver a large amount of cargo into tumor cells via TfR1-mediated specific binding followed by rapid internalization[19–22].
- Excellent biocompatibility. HFn nanocages exist naturally in humans and do not contain any potentially toxic elements that would activate the inflammatory or immunological responses; thus, they display a natural safety profile[17,23].

[1]Experimental Center of Advanced Materials, School of Materials Science & Engineering, Beijing Institute of Technology, Beijing, China. [2]Department of Nuclear Medicine, Zhongshan Hospital, Fudan University/Shanghai Institute of Medical Imaging, Shanghai, China. [3]Institute of Biophysics, Chinese Academy of Sciences, Beijing, China. [4]These authors controibuted equally: Jianlin Zhang, Dengfeng Cheng, Jiuyang He. ✉e-mail: mmliang@bit.edu.cn

Table 1 | Examples of preparation and applications of HFn-based formulations

HFn nanocage	Loaded cargo	Loading method	Application	Ref
Recombinant human HFn	Cisplatin	pH	Targeting drug delivery and tumor targeting therapy	51,52
Recombinant human HFn	Oxaliplatin	pH	Tumor targeting therapy	53
Recombinant human HFn	Paclitaxel	pH	Conjugated with nanobody for targeted photodynamic therapy	54
Recombinant human HFn	Doxorubicin	Diffusion	Targeting drug delivery	13
Recombinant human HFn	Photodynamic reagents	pH	By conjugating with nanobody for targeted drug delivery	54
Recombinant human HFn	SiRNA and miRNA	Chemical conjugation	Genetically modified ferritin with targeting ability to enhance efficiency and safety of the delivery system to cancer cells	55
Recombinant human HFn	SpyTag-fused antigens	Chemical conjugation	Antitumor immunity	56
Recombinant human HFn	Photosensitizers (zinc hexadecafluorophthalocyanine)	Diffusion	Efficient photodynamic therapy against cancer	37
Recombinant human HFn	Mitoxantrone	pH	Tumor (colon, breast, sarcoma and pancreas) therapy	57
Recombinant human HFn	Gefitinb	Diffusion	Drug delivery	38
Recombinant human HFn	IR820	pH	Multimodal imaging-guided photothermal therapy	58
Recombinant human HFn	β-carotene	pH	Encapsulate the lipid-soluble compound for food chemistry applications	59
Recombinant human HFn	Sinoporphyrin sodium	pH	Photothermal and photodynamic co-therapy	60
Recombinant human HFn	Fe, dysprosium, Gd^{3+}, Mn^{2+}	Diffusion	MRI imaging for tumor diagnostics	39,61–63
Recombinant human HFn	DTPA-chelated gadolinium, gadolinium oxide (Gd_2O_3) NPs	Chemical conjugation	MRI imaging	64,65
Recombinant human HFn	^{99m}Tc-HFn	Chemical conjugation	Combined SPECT and CT imaging for precise tumor diagnostics	66
Recombinant human HFn	Iron oxide NP in the interior cavity and ^{125}I radionuclide conjugation on the surface	Chemical conjugation	SPECT/MRI imaging for more precise tumor detection	19
Recombinant human HFn	Cy5.5 modified on the surface and ^{64}Cu loaded in the interior cavity	pH	PET/NIRF imaging for more precise tumor detection	32
Recombinant human HFn	Co_3O_4	Diffusion	Modified with specific targeting peptide of hepatocellular carcinoma (HCC) tumor tissue for HCC prognostic diagnosis	67
Recombinant human HFn	Iron oxide NPs	Diffusion	Encapsulating iron oxide NPs for targeting and visualizing tumour tissues	11
Recombinant human HFn	Gold NPs	Diffusion	Used as a template for NP synthesis	68
Horse spleen apoferritin	CuS, CuFe	Diffusion, urea-based	Semiconductor, magnetic	69,70
Horse spleen apoferritin	Co and its oxide NPs	Diffusion	Chemical catalyst, biosensors	71–73
Horse spleen apoferritin	CoPt, CoNi	Diffusion	Data storage, bimetallic NP synthesis	74,75
Horse spleen apoferritin	Ni	Diffusion	Magnetic materials	71,76
Horse spleen apoferritin	Iron phosphate, iron arsenate, iron molybdate and iron vanadate	Diffusion	Chemical synthesis	77
Horse spleen apoferritin	Au-Ag alloy NPs	Diffusion	Alloy NP synthesis	78
Horse spleen apoferritin	Ag NPs	Diffusion	Antimicrobial and catalytic materials	79,80
Horse spleen apoferritin	Pb and its compounds	pH	Biosensor and bioimaging	81–84
Horse spleen apoferritin	YPO_4	Diffusion	Cancer radioimmunotherapy	85
Horse spleen apoferritin	$LuPO_4$	Diffusion	Functionalized nanomaterial synthesis	86
Horse spleen apoferritin	$CaCO_3$, $SrCO_3$, $BaCO_3$ and $Ca_3(PO_4)_2$	Diffusion	Basic loading studies	87
Horse spleen apoferritin	Prussian blue	Diffusion	Biological detection	88
Horse spleen apoferritin	Cr hydroxide	Diffusion	Nanoelectronics	76

Table continued

Table 1 (continued)

HFn nanocage	Loaded cargo	Loading method	Application	Ref
Horse spleen apoferritin	U and its oxide NPs	pH	Neutron-capture therapy	89
Horse spleen apoferritin	Cisplatin	pH	Targeting drug delivery and tumor targeting therapy	51,90
Horse spleen apoferritin	Doxorubicin	pH	Inlaying radiosensitizer for imaging guided tumor therapy and develop drug delivery system	91,92
Horse spleen apoferritin	Curcumin	pH	Drug delivery with curcumin capsulation to prevent hepatocellular damage	93
Horse spleen apoferritin	Neural drugs, such as carbachol and atropine	Urea-based	Regulate the nervous microenvironment to control pancreatic cancer progression	94
Horse spleen apoferritin	CeO_2	pH	Ameliorating ROS-scavenging activity	45
Horse spleen apoferritin	Platinum NPs	Diffusion	Chemical catalyst	40
Horse spleen apoferritin	ZnSe, CdS, CdSe	Diffusion	Used as a template for NP synthesis	46–48
Horse spleen apoferritin	TiO_2	Diffusion	Chemical catalyst	49
Recombinant rat HFn	Copper sulfide NPs	Diffusion	Cancer photothermal therapies	31
Recombinant Listeria innocua ferritin	Co and its oxide NPs	Diffusion	Chemical catalyst, biosensors	50

- Universal vehicle system. The methods for cargo encapsulation within HFn nanocages are universal and capable of accurately controlling drug loading, and precisely adjusting the formed nanocores within HFn nanocages[24–27].
- Easy scaling-up procedure. HFn vehicles are efficiently produced in *Escherichia coli* with a high yield and cargo payload efficiency[11,28].
- Definite pharmacokinetics. Compared with artificial nanocarriers, HFn vehicles show definite in vivo behavior due to the well-defined morphology and surface physicochemical properties[29–32]. In particular, the 12 nm diameter of HFn nanocage morphology is capable of overcoming the biophysical barriers posed by tumor microenvironment and penetrating deep into tumors[33,34].

It has been widely reported that the mechanism of intracellular release of cargoes is through the specific binding of human HFn to TfR1, which is often overexpressed on tumor cells[11,17]. Binding to TfR1 leads to endocytosis of HFn with subsequent trafficking of HFn into lysosomes, followed by disassembly of HFn nanocages and cargo release into the acidic environment of lysosomes[17]. Several groups have further functionalized human HFn with specific ligands such as peptides (e.g., RGD)[28] and growth factors (e.g. epidermal growth factor)[35] to improve targeting to tumor cells. Horse spleen ferritin, which is mostly composed of L subunits, has also been used as nanocarrier for drug delivery studies through Scara5-mediated tumor cell recognition and uptake[36]. In this protocol, we describe the use of human HFn to encapsulate controlled amounts of cargo. The resulting formulations can be used in further studies to target delivery to tumors in vivo.

The unique nanocage structure has been previously demonstrated to provide excellent biocompatibility, intrinsic tumor-targeting capability and favorable in vivo pharmacokinetics, thus enabling HFn vehicles to target therapeutic drugs and diagnostic molecules to the therapeutic target (Table 1).

Strategies for loading ferritin nanocages

To date, many methods have been developed to optimize loading of cargo within ferritin nanocages (Table 1). There are three main methods usually used for ferritin-based cargo loading: diffusion methods, pH/urea-based ferritin disassembly/reassembly methods and thermal response channel-based methods (Table 1). Each method has intrinsic advantages and limitations, and the optimal method is dependent on the type of cargo. Therefore, to achieve a high efficiency of cargo loading, we recommend choosing the most appropriate method based on the physicochemical properties of the cargo being loaded.

The diffusion method requires the structure of the ferritin nanocage to remain intact during loading; thus, only limited numbers of small molecule cargoes (with size < 5 Å)[37,38] and metal ions

(such as Pt^{2+}, Cu^{2+}, Mn^{2+}, etc.)[39,40] can be loaded into ferritin nanocages, and this must be through the ion channel at the threefold axis of ferritin.

The urea or pH-based disassembly/reassembly methods allow the loading of large cargoes into the cavity of ferritin nanocages by reversibly disassembling and reassembling ferritin nanocages via adjusting pH or urea levels of reaction solution. Usually, ferritin nanocages completely dissociate at pH < 2.0 or pH > 12.0, which often results in the formation of holes in the nanocage of ferritin after reassembly[41,42]. The urea-based disassembly/reassembly method was therefore developed to gently disassemble and reassemble ferritin nanocages and avoid the formation of defects. However, the urea-based method takes much more time to accomplish the encapsulating process (~3 d) compared with the pH-based method (~ 1 d) because it requires sequential dialysis in gradient concentrations of urea solution to reassemble HFn nanocages, which takes ~24 h (for example, Step 4 of Procedure 2).

The threefold hydrophilic channel on the ferritin nanocage opens when heated to 60 °C. The thermal response channel-based method was thus designed to allow the cargoes to enter the cavity of ferritin via the opened channel (for example, Steps 3 and 4 of Procedure 3).

In this protocol, we use the thermal response channel-based method to accelerate loading of $^{64}Cu^{2+}$ or Gd^{3+} ions through the ion channel at the threefold axis of ferritin. We also describe how to genetically modify the inner surface of the ferritin cavity using 8 × His to chelate the entered $^{64}Cu^{2+}$ or Gd^{3+} ions at the His sites within the cavity (Step 4 of Procedure 3, Steps 2 and 3 of Procedure 4).

Limitations of the protocol

Over the past decade, a broad variety of cargo molecules, including drugs, imaging agents, therapeutic genes and metal NPs have been encased in the cavity of ferritin nanocages for a broad range of biomedical applications[25,29,43,44]. The protocol described here specifically presents approaches to synthesize Fe_3O_4, Co_3O_4 or MnO_2 NPs within the cavity of a wild-type human HFn nanocage, and provides the procedures for loading doxorubicin, radioisotopes and Gd^{3+} within His-tag genetically engineered or wild-type human HFn nanocages. Since genetic engineering with different functional groups changes the physicochemical properties of ferritin nanocages, the procedure described here must be further developed and modified to be suitable for ferritin nanocages engineered to have different modifications. Preparation of other metal oxide NPs or loading of other drugs and metal ions within HFn nanocages has not been attempted in our laboratory using this protocol. In this protocol, the capture of Gd^{3+} and $^{64}Cu^{2+}$ ions within HFn nanocages is achieved through the chelate interaction of the fused His-tag on the interior surface of HFn. Hence, this method is applicable only to the metal ions with high His-tag affinity such as Ni^{2+}, Co^{2+}, Cu^{2+}, Ca^{2+}, Fe^{3+}, Gd^{3+}, etc.

When selecting the optimal method of loading cargo, feasibility of scale-up for clinical applications should be considered. The production and purification characteristics of HFn and His-tag fused HFn permit manufacturing to be robustly and reproducibly scaled up. In addition, the encapsulation method of doxorubicin, radioisotopes and Gd^{3+} within the human HFn nanocages is also simple and can easily be scaled up while retaining high cargo payload efficiency. However, preparation of the metal oxide NPs within the HFn nanocage is performed in a glove box under an N_2 atmosphere to maintain atmospheric purity at <600 ppm oxygen. This requirement severely limits the feasibility of scaling up this specific application. In addition, the nanoparticle nucleation and growth process within the cavity of HFn nanocage are highly sensitive to reaction conditions. Thus, stationary reaction temperature, pH and precise titrating of metal ions and H_2O_2 are required to form the homogeneous nanoparticle within the HFn nanocage.

Experimental design

In this protocol, we present four alternative step-by-step procedures that allow researchers to encapsulate metal oxide NPs, antitumor drug doxorubicin, contrast agent Gd^{3+} or radioisotope $^{64}Cu^{2+}$ within the interior cavity of a human HFn nanocage (Table 2):

- Procedure 1: synthesis of Fe_3O_4, Co_3O_4 or MnO_2 NPs within the interior cavity of a wild-type human HFn nanocage under an N_2 atmosphere.
- Procedure 2: loading of doxorubicin into the cavity of a wild-type human HFn nanocage through the disassembly of a HFn nanocage in urea in the presence of doxorubicin, followed by reassembly by a series of stepwise gradients of urea.
- Procedure 3: loading of Gd^{3+} into the cavity of a genetically engineered human HFn nanocage.
- Procedure 4: loading of $^{64}Cu^{2+}$ radioisotope into the cavity of a genetically engineered human HFn nanocage.

Table 2 | Flowchart of the protocol

Protocol stages	Metal oxide NPs (Procedure 1)	Doxorubicin (Procedure 2)	$Gd^{3+}/^{64}Cu^{2+}$ (Procedure 3/4)
Preparation	Prepare oxygen-free atmosphere and degassed solutions (Steps 1–4)	Prepare HFn and doxorubicin stock solutions ('Reagent setup')	Prepare HFn-His and $Gd^{3+}/^{64}Cu^{2+}$ stock solutions ('Reagent setup')
Reaction	Mineralization of metal ions within HFn nanocages (Steps 5–11)	Dis- and reassembly of HFn to encapsule doxorubicin inside (Steps 1–5)	Open the threefold hydrophilic channel of the ferritin nanocage by heating to 60 °C to capture $Gd^{3+}/^{64}Cu^{2+}$ inside (Steps 1–4/1–3)
Product collection	Collect the mineralized HFn (Steps 12 and 13)	Collect the HFn-encapsulated doxorubicin (Step 6)	Collect the $Gd^{3+}/^{64}Cu^{2+}$-loaded HFn-His (Steps 5–6/4)
Quantification	Quantification of the mineralized HFn (Steps 14 and 15)	Quantification of HFn-encapsulated doxorubicin (Steps 7 and 8)	Quantification of HFn-His-captured $Gd^{3+}/^{64}Cu^{2+}$ (Steps 7/5)

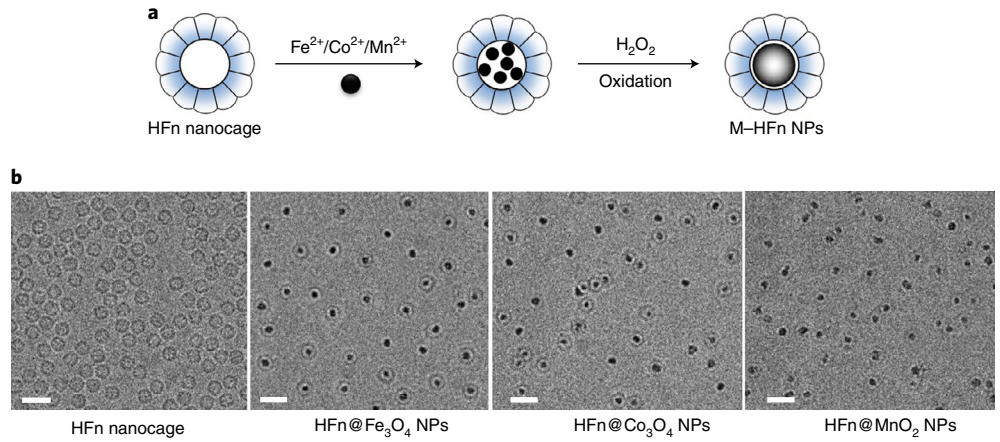

Fig. 1 | Characterization of HFn encapsulation of metal oxide NPs. a, Schematic representation of HFn encapsulation of metal oxide NPs (M–HFn). **b**, Cryo-EM images of HFn nanocages and M–HFn NPs. Scale bar, 20 nm. For details of how to perform cryo-EM characterization, please refer to the Supplementary Methods.

The choice of approach must be determined by the physicochemical properties of the cargo. For metal oxide nanoparticle preparation within the HFn nanocage, we first load metal ions into the interior cavity of HFn nanocage via the channel formed at the interface between subunits, followed by oxidation with hydrogen peroxide into metal oxide nanoparticle at the ferroxidase sites within the cavity (Fig. 1). For doxorubicin loading, we disassemble HFn nanocages in urea solution and load doxorubicin into the interior cavity of HFn while reassembling HFn nanocages using a series of stepwise gradients of urea (Fig. 2). For $^{64}Cu^{2+}$ and Gd^{3+} ions loading, we first genetically modify the inner surface of the ferritin cavity using 8 × His, and then chelate the entered $^{64}Cu^{2+}$ or Gd^{3+} ions at the His sites within the cavity (Fig. 3).

Encapsulation of metal oxide NPs within the HFn nanocage (Procedure 1)

Metal oxide NPs are synthesized directly within the cavity of HFn nanocage. Oxygen-free reaction conditions must be strictly maintained. We describe how this can be achieved in a glove box under an N_2 atmosphere (Steps 1–11) plus how to collect and quantify the mineralized HFn (Steps 12–15). The reaction atmosphere must be oxygen-free so that the loaded metal ions can be controllably oxidized by the precisely dosed H_2O_2. The formed nanocores within human HFn can thus be adjusted via the dosing speed and duration of metal ions and H_2O_2.

Encapsulation of doxorubicin within the HFn nanocage (Procedure 2)

Doxorubicin is gradually loaded while the HFn nanocage is disassembled in 8 M urea (Steps 1–3) and then slowly reassembled by dialysis against the gradient concentrations of urea solution (Steps 4 and 5). We recommend using no less than five different gradient concentrations of urea solution

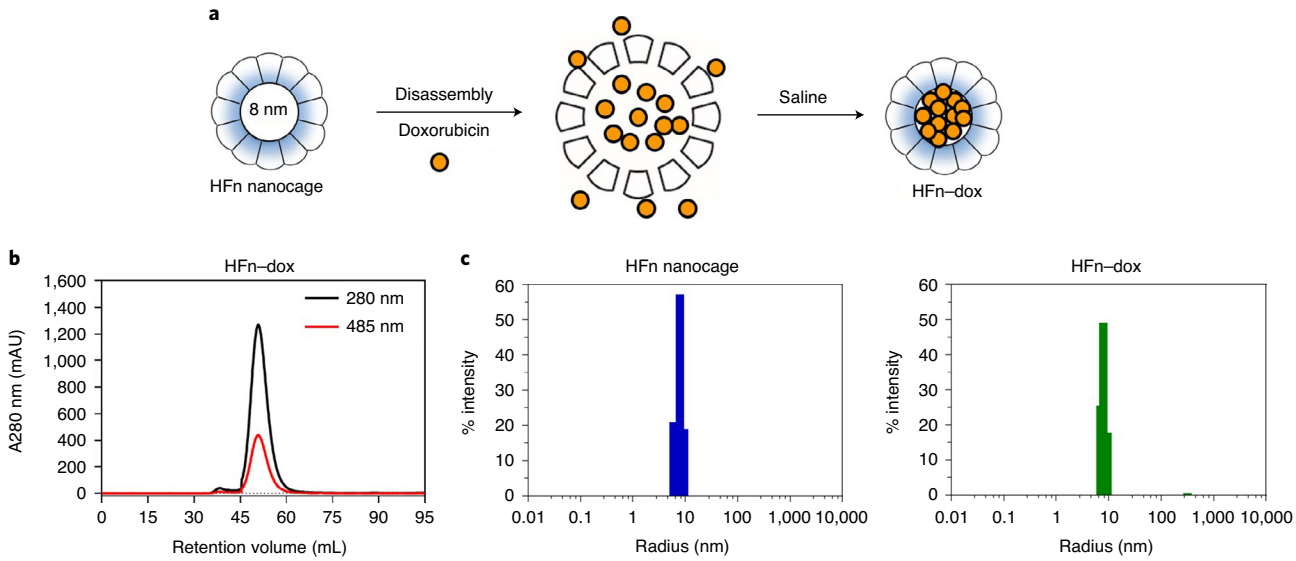

Fig. 2 | Characterization of HFn nanocage encapsulation of doxorubicin (Dox). a, Schematic representation of the Dox loading process. **b**, Representative SEC analysis of Dox-loaded HFn nanocages (HFn–Dox) by in-line UV detection at 280 nm (HFn) and 485 nm (Dox). **c**, DLS analysis of HFn nanocage (left) and HFn–Dox (right). For details of how to perform SEC and DLS analysis, please refer to the Supplementary Methods.

(for example, 7, 5, 3, 2, 1 and 0 M, each for 4 h) to ensure the assembly process of HFn nanocages is carried out gently and gradually. Generally, this process is time-consuming but gentle enough to keep HFn spherical structure intact. Successful encapsulation of doxorubicin is determined quantitatively by measuring the absorbance at 485 nm.

Encapsulation of $Gd^{3+}/^{64}Cu^{2+}$ within the HFn nanocage (Procedures 3 and 4)

Detailed instructions are provided for the encapsulation of $Gd^{3+}/^{64}Cu^{2+}$ ions within the HFn nanocage. The hydrophilic threefold channels on ferritin nanocages open when the temperature reaches 60 °C, which allows the $Gd^{3+}/^{64}Cu^{2+}$ ions in solution to enter the cavity of ferritin via the opened channels and then be captured by the genetically fused His-tag within the inner surface of the ferritin cavity. Once the temperature drops below 60 °C, the channels of ferritin close and the ions remain encapsulated within the cavity of the HFn nanocage. Since the capture of Gd^{3+} and $^{64}Cu^{2+}$ ions within HFn nanocages is achieved through chelation of the fused His-tag on the interior surface of HFn, this method can only be applied to metal ions with high His-tag affinity such as Ni^{2+}, Co^{2+}, Cu^{2+}, Ca^{2+}, Fe^{3+}, Gd^{3+}, etc.

Because $^{64}Cu^{2+}$ has a short half-life (12.7 h), it is important to reduce the number of preparation steps and overall production and purification time of $^{64}Cu^{2+}$-loaded HFn. In particular, we recommend using column filtration to remove free $^{64}Cu^{2+}$, which requires substantially less time than other methods such as dialysis to purify the radio-loaded biomolecules.

Materials

Reagents

- pET-30a (+) plasmid (Novagen, cat. no. 69909-3)
- *Escherichia coli* BL21 (DE3) (TransGen Biotech, cat. no. CD601-02)
- NaCl (Sinopharm Chemical Reagent, cat. no. 10019308)
- Yeast extract (Oxoid, cat. no. LP0021)
- Tryptone (Oxoid, cat. no. LP0042)
- Kanamycin sulfate (Merck, cat. no. 5880)
- Isopropyl-β-D-thiogalactopyranoside (IPTG; TransGen Biotech, cat. no. GF101-01)
- Ammonium sulfate (Sinopharm Chemical Reagents, cat. no. 10002918)
- Trizma base (VETEC, cat. no. V900483)
- HCl (Sinopharm Chemical Reagents, cat. no. 10011018) **!CAUTION** Causes severe burns. Do not inhale the vapor. Avoid contact with eyes, skin and clothing. Avoid prolonged or repeated exposure. Use in a fume hood and wear gloves, protective eyewear and a laboratory coat.

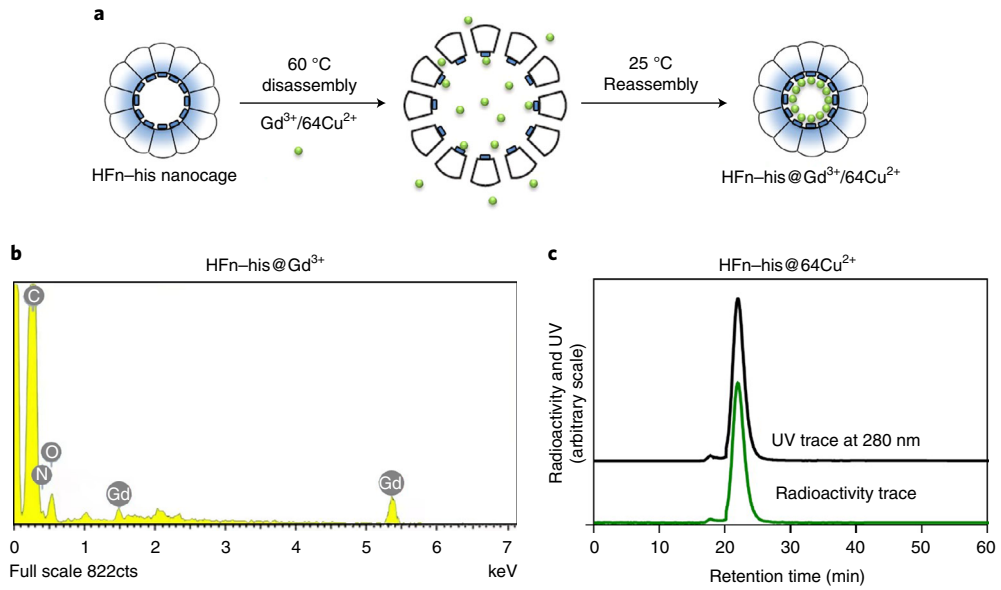

Fig. 3 | Characterization of HFn–His nanocage encapsulation of Gd^{3+} or $^{64}Cu^{2+}$. a, Schematic representation of the Gd^{3+} or $^{64}Cu^{2+}$ loading within HFn–His nanocages. The inner surface of the cavity of the ferritin was genetically modified with 8 × His to chelate the loaded $^{64}Cu^{2+}$ or Gd^{3+} ions. **b**, Area-scan energy-dispersive X-ray spectroscopy analysis of HFn–His@Gd^{3+}. **c**, Size-exclusion HPLC analyses of HFn–His@$^{64}Cu^{2+}$. For details of how to perform energy-dispersive X-ray spectroscopy and size-exclusion HPLC analysis, please refer to the Supplementary Methods.

- Na_2HPO_4 (Sinopharm Chemical Reagents, cat. no. 20040617)
- KH_2PO_4 (Sinopharm Chemical Reagents, cat. no. 10017608)
- KCl (Sinopharm Chemical Reagents, cat. no. 10016308)
- BCA protein assay kit (Pierce, cat. no. 23225)
- HNO_3 (Sinopharm Chemical Reagents, cat. no. 7697-37-2) **! CAUTION** Causes severe burns. Do not inhale the vapor. Avoid contact with eyes, skin and clothing. Avoid prolonged or repeated exposure. Use in a fume hood and wear gloves, protective eyewear and a laboratory coat.

Equipment

- Thermostat water bath (LICHEN, model no. HH-2)
- Autoclave (Beijing Faen Scientific & Trading, model no. D-1-70)
- Horizontal laminar flow clean bench (ESCO, model no. LVG-6AG-S8)
- Incubator shaker (CRYSTAL, model no. IS-RDH1)
- Avanti J-E centrifuge (Beckman Coulter, model no. 369001)
- Ultrasonic cell crusher (Shanghai HUXI, model no. JY96-IIN)
- Multifuge X1R centrifuge (Thermo Fisher, model no. 75004250)
- Magnetic stirrer (LICHEN, model no. LC-SMS-HS)
- Ultrapure water system (Merck, model no. Milli-Q Advantage A10)
- Dialysis bag (viskase, cat. no. MD34-14)
- 0.22 μm sterile filter (Sartorius, cat. no. FF342-10pcs)
- Suction filtration apparatus composed of a vacuum pump (JINTENG, model no. GM-2), a filtration container (JINTENG, model no. T-50.1L) and 0.2 μm filtration membrane (JINTENG, model no. φ 50 mm/0.2 μm/MCE).
- AKTA avant 150 (General Electric, model no. 28-9308-42)
- HiTrap Q FF 5 mL prep grade anion exchange chromatography column (General Electric, cat. no. 17-5156-01)
- Vivaspin 20 ultrafiltration tube (Sartorius, cat. no. VS2042-1)
- HiLoad 16/600 Superdex 200 prep grade size exclusion chromatography (SEC) column (General Electric, cat. no. 28-9893-35)
- 96-well microplates (Beyotime, cat. no. FPT010)
- Microplate reader (Thermo, model no. Multiskan SkyHigh)

Reagent setup

LB medium

Dissolve 10 g typtone, 5 g yeast extract and 10 g NaCl in 1 L of deionized water, and then autoclave the solution at 121 °C for 15 min. The obtained sterilized LB medium can be stored at room temperature (RT, 25 °C) for 3 months.

Kanamycin sulfate solution

Dissolve kanamycin sulfate in deionized water to a final concentration of 50 mg/mL. Sterilize the kanamycin sulfate solution using a 0.22 μm sterile filter on a horizontal laminar flow clean bench. The sterilized kanamycin sulfate solution can be stored at −80 °C for 3 months.

IPTG solution

Dissolve IPTG in deionized water to a final concentration of 1 M. Sterilize the IPTG solution using a 0.22 μm sterile filter on a horizontal laminar flow clean bench. The sterilized IPTG solution can be stored at −80 °C for 3 months.

Tris-HCl/NaCl buffer

Dissolve Trizma base in deionized water to a final concentration of 200 mM, and adjust the final pH to 8.0 using HCl. The obtained 200 mM Tris-HCl (pH 8.0) buffer can be stored at RT for 3 months. Dilute 200 mM Tris-HCl (pH 8.0) buffer with deionized water to obtain 50 mM Tris-HCl (pH 8.0) buffer and 20 mM Tris-HCl (pH 8.0) buffer. Dissolve NaCl in 20 mM Tris-HCl (pH 8.0) buffer to obtain 20 mM Tris-HCl containing 1 M NaCl (pH 8.0) buffer. ▲**CRITICAL STEP** Tris-HCl (pH 8.0) buffer should be suction filtrated freshly with 0.2 μm membrane before flowing into the chromatography columns.

Phosphate-buffered saline (PBS)

Dissolve 8.0 g NaCl, 0.2 g KCl, 1.44 g Na_2HPO_4 and 0.24 g KH_2PO_4 in 800 mL deionized water, and adjust the final pH to 7.4 using HCl. Add deionized water to make the solution volume up to 1,000 mL. Filter-sterilize (0.22 μm), and store PBS solution at 4 °C for no more than 6 months.

HFn and HFn–His nanocages

The recombinant human HFn and HFn–His are expressed in *Escherichia coli* BL21(DE3) where they self-assemble into the 24 subunit nanocages. The inner surface of HFn–His contains exposed 8 × His, which is used to chelate the loaded $^{64}Cu^{2+}$ or Gd^{3+} ions. The nucleotide sequence for encoding HFn is from the National Center for Biotechnology Information (CCDS41655.1), and the nucleotide sequence for encoding HFn–His was designed by inserting an 8 × His with the linker of GSGGG (5′-GGT AGC GGC GGT GGC CAT CAC CAT CAT CAC CAC CAT CAC-3′) at the 3′-terminus before the stop codon. The following procedure can be followed to generate the nanocages:

1 Synthesize the nucleotide sequences of HFn and HFn–His (we use sequences synthesized by Shanghai Generay Biotech). During synthesis, introduce a NdeI restriction site to the 5′-terminus and a BamHI restriction site to the 3′-terminus.
2 Separately insert the synthesized genes to replace the nucleotide sequence between the NdeI and BamHI restriction sites of the pET-30a(+) plasmid.
3 Separately transform the obtained HFn-pET-30a (+) plasmid and HFn–His-pET-30a (+) plasmid into *Escherichia coli* BL21(DE3) cells using the Escherichia coli BL21 (DE3) kit (TransGen Biotech, cat. no. CD601-02) following the manufacturer's instructions.
4 Grow *Escherichia coli* cells (BL21(DE3)) containing plasmid HFn-pET-30a (+) or HFn–His-pET-30a (+) in LB medium containing kanamycin (50 μg mL^{-1}) in a shaking flask at 37 °C.
5 Once growth reaches an OD 600 of 0.6, induce expression of plasmid-encoded proteins by adding 0.5 mM IPTG and switching the culture temperature to 25 °C.
6 Incubate *Escherichia coli* BL21(DE3) cells in a shaking flask (220 rpm) for another 12 h.
7 Centrifuge cells at 4,000*g* for 30 min at 4 °C, discard supernatant and resuspend the precipitate in 50 mM Tris-HCl buffer (pH 8.0) to a final concentration of 10% (wt/vol). Sonicate the solution on ice (220 w, periodic working for 2 s and resting for 2 s, total working for at least 20 min), followed by centrifugation at 12,000*g* for 30 min at 4 °C to remove debris.

Discard pellet. ▲ **CRITICAL** Protease inhibitors are not used in this protocol because the BL21 (DE3) cells are deficient in Lon protease and OmpT protease. A typical yield is between 50 and 100 mg of HFn or HFn–His per 1 L bacterial lysate even without the use of protease inhibitors. In addition, DNAse/RNAase are not required because any contaminating DNA/RNA is efficiently removed by ammonium sulfate precipitation and the following anion exchange chromatography.

8 Heat the supernatant to 70 °C for 15 min, and then centrifuge at 12,000*g* for 30 min to remove the heat-precipitated *Escherichia coli* host proteins. Discard pellet.

9 Precipitate the protein gradients in the supernatant by adding ammonium sulfate (53%, wt/vol) to the supernatant. Stir the mixture at RT for 2 h to ensure the protein gradients are thoroughly precipitated.

10 Centrifuge the mixture at 12,000*g* for 30 min (4 °C) to collect the protein precipitate, and then redissolve it using 20 mM Tris-HCl buffer (pH 8.0).

11 Dialyze the protein solution against 20 mM Tris-HCl (pH 8.0) overnight to remove the remanent ammonium sulfate gradient.

12 Load the dialyzed protein solution onto a Q Sepharose Fast Flow anion exchange chromatography column (column volume 5 mL), with the mobile phase composed of 20 mM Tris-HCl (pH 8.0) buffer and 20 mM Tris-HCl buffer (pH 8.0, 1 M NaCl) buffer.

13 Collect the eluted portion with a conductivity value between 20 mS/cm and 40 mS/cm.

14 Concentrate the collection with an ultrafiltration tube.

15 Load the concentrated protein solution onto a HiLoad 16/600 Superdex 200 prep grade SEC column (column volume 120 mL) with 40 mM Tris-HCl (pH 8.0, 200 mM NaCl) buffer as the mobile phase to purify the HFn and HFn–His proteins. Approximately 55 mL pure HFn or HFn–His protein should elute. ▲ **CRITICAL** The use of gel-filtration chromatography is not suitable for industrial manufacture owing to it being time consuming, expensive and requiring a large size of columns. Scale-up of the purification process to meet the demands of industrial manufacture while maintaining the quality of HFn/HFn–His protein can be achieved by using hydrophobic chromatography to replace the SEC. Anion exchange chromatography combined with hydrophobic chromatography can achieve a protein purification purity of >95 %. In particular, both anion exchange chromatography and hydrophobic chromatography are highly efficient for industrial applications.

16 Dissolve the obtained HFn and HFn–His proteins in 20 mM Tris-HCl (pH 8.0, 100 mM NaCl, 30% glycerin).

17 Determine the final protein concentration by BCA Protein Assay Kit.

■ **PAUSE POINT** Store HFn and HFn–His proteins at 4 °C for a maximum of 6 months or at −80 °C for up to 3 years. Samples stored at 4 °C should undergo 0.22 μm filtration prior to storage to remove bacterial contamination. In addition, it is preferable to divide the HFn and HFn–His into aliquots before freezing to avoid unnecessary freezing and thawing.

? TROUBLESHOOTING

Additional materials required for Procedure 1

Reagents

- Sodium hydroxide (Sigma-Aldrich, cat. no. S8045)

  ! CAUTION Sodium hydroxide is highly irritating upon contact with eyes or skin; it should be handled with gloves.
- Hydrogen peroxide 30% (wt/vol) aqueous solution (Sinopharm Chemical Reagent Beijing, cat. no. 10011208)

  ! CAUTION Hydrogen peroxide is highly irritating to eyes, skin and upon ingestion, and should be handled with gloves under a fume hood.
- Trisodium citrate dihydrate (Sinopharm Chemical Reagent, cat. no. 10019408)
- $(NH_4)_2Fe(SO_4)_2 \cdot 6H_2O$ (Sigma-Aldrich, cat. no. 203505)
- $Co(NO_3)_2 \cdot 6H_2O$ (Sigma-Aldrich, cat. no. 203106)
- $MnCl_2 \cdot 4H_2O$ (Sigma-Aldrich, cat. no. 203734)

Equipment

- Anaerobic glove box (Plas Labs, model no. 800-866-7527)
- O_2 Transmitter (Advanced Instruments, model no. GPR-1500)

- IKA RCT basic IKAMAG safety control hot plate magnetic stirrer (Aldrich, model no. Z645060) equipped with IKA ETS-D5 temperature controller (Aldrich, model no. Z645125)
- Dosing device 800 Dosino (Metrohm, model no. 28000010) connected with 902 Titrando (Metrohm, model no. 29020010)

Equipment setup

Thermostatic water bath

We create a thermostatic water bath with stirring by using a magnetic stirrer equipped with a temperature controller. Set in a beaker of water that has been preheated to thermostatic 65 °C.

Additional materials required for Procedure 2

Reagents

- Doxorubicin hydrochloride (Sangon Biotech, cat. no. A603456)
- Urea (Sinopharm Chemical Reagent, cat. no. 10023218)

Equipment

- NanoDrop UV-Vis spectrophotometer (Thermo Fisher Scientific, model no. NanoDrop 2000/2000c)

Reagent setup

Urea solution

Dissolve urea in deionized water to a concentration of 8 M, 7 M, 5 M, 3 M, 2 M and 1 M, respectively. Filter-sterilize (0.22 μm), and store them at 4 °C for no more than 6 months.

Doxorubicin stock solution

Dissolve doxorubicin hydrochloride in deionized water to a final concentration of 10 mg/mL. Filter-sterilize (0.22 μm), and store it at 4 °C for no more than 1 month.

▲ **CRITICAL** The prepared solution should be handled in the dark.

Additional materials required for Procedure 3

Reagents

- $Gd(NO_3)_3 \cdot 6H_2O$ (Innochem, cat. no. A10171)

Reagent setup

Gadolinium ion stock solution

Dissolve $Gd(NO_3)_3 \cdot 6H_2O$ in deionized water to a final concentration of 480 mM. Filter-sterilize (0.22 μm), and store them at 4 °C for no more than 6 months.

Equipment

- IKA RCT basic IKAMAG safety control hot plate magnetic stirrer (Aldrich, model no. Z645060) equipped with IKA ETS-D5 temperature controller (Aldrich, model no. Z645125)
- Dosing device 800 Dosino (Metrohm, model no. 28000010)

Reagent setup

Gadolinium ion stock solution

Dissolve $Gd(NO_3)_3 \cdot 6H_2O$ in deionized water to a final concentration of 480 mM. Filter-sterilize (0.22 μm), and store at 4 °C for no more than 6 months.

Equipment setup

Thermostatic water bath

A thermostatic water bath with stirring can be created using the magnetic stirrer equipped with the temperature controller. Set in a beaker of water preheated to thermostatic 60 °C.

Additional materials required for Procedure 4

Equipment

- Biomedical cyclotron (Sumitomo Heavy Industrials, model no. HM-20)
- PD-10 desalting columns (GE Healthcare Life Sciences, cat. no. 17-0851-01)

Reagent setup

$^{64}Cu^{2+}$ ion solution

Obtain freshly prepared $^{64}Cu^{2+}$ ions from a biomedical cyclotron via the ^{64}Ni (p, n) ^{64}Cu reaction. **! CAUTION** As with all radionuclides emitting penetrating radiation, standard shielding and radionuclide handling procedures must be employed with $^{64}Cu^{2+}$ ions. Direct exposure to the radioactivity should be kept to a minimum. Individuals working with the radioisotope should monitor their radiation exposure with appropriate devices.

Equipment setup

Thermostatic water bath

We establish a thermostatic water bath with stirring by using a magnetic stirrer equipped with a temperature controller. Set in a beaker of water preheated to thermostatic 60 °C.

Procedure 1: preparation of metal oxide NPs within the HFn nanocage ● Timing ~5 h

▲ CRITICAL This section describes how to prepare Fe_3O_4, Co_3O_4 or MnO_2 NPs within the HFn nanocage. We have not prepared other metal oxide NPs within the HFn nanocage; thus, adjustments might be required if using alternative metal oxides.

1 Degas 2 L of deionized water by boiling it for at least 30 min, and keep the degassed water in an airtight flask with no air inside.

2 Transfer 1 mL HFn stock solution (10 mg/mL in 20 mM Tris-HCl, pH 8.0, containing 100 mM NaCl and 30% glycerin), 0.1 mL H_2O_2 stock solution (30% (wt/vol) aqueous solution), NaCl (1.1688 g), NaOH (0.2 g), sodium citrate (8.823 g), 50, 200 and 500 mL vials, degassed water, 50 and 100 mL cylinder, pipette and pipette tips to a glove box before use. Also transfer $(NH_4)_2FeSO_4$ (0.49 g), $Co(NO_3)_2$ (0.3638 g) or $MnCl_2$ (0.2474 g).
▲ CRITICAL STEP Fresh H_2O_2 should be used to minimize H_2O_2 decomposition. The H_2O_2 stock solution bottle (30% (wt/vol) aqueous solution from Sigma) should not be used for more than 1 month after opening.

3 Exchange the air in glove box with N_2 to maintain the atmosphere purity at <600 ppm oxygen.
▲ CRITICAL STEP The reaction should be carried out under N_2 atmosphere with oxygen <600 ppm to avoid generating precipitates during the experiment. Precipitates are generated by oxidation of Fe^{2+} by dissolved oxygen.
? TROUBLESHOOTING

4 Prepare the following solution using degassed deionized water: 200 mL NaCl (100 mM), 100 mL NaOH (50 mM), 100 mL H_2O_2 (4.17 mM), 100 mL sodium citrate (300 mM) and 100 mL of either $(NH_4)_2FeSO_4$ (12.5 mM), $Co(NO_3)_2$ (12.5 mM) or $MnCl_2$ (12.5 mM).
▲ CRITICAL STEP The above solution should be freshly prepared in degassed deionized water in glove box under N_2 atmosphere.
▲ CRITICAL STEP Fresh H_2O_2 should be used to minimize H_2O_2 decomposition.

5 Place 40 mL of NaCl solution (100 mM in degassed water) into the reaction vial.

6 Maintain the reaction vial at 65 °C using a thermostatic water bath.

7 Add HFn stock solution to the reaction vial to a final concentration of 0.25 mg/mL.
▲ CRITICAL STEP The protein concentration should not be increased to more than 1 mg/mL to avoid protein precipitation at high concentrations during the mineralization process.

8 Simultaneously add the prepared metal source ($(NH_4)_2FeSO_4$, $Co(NO_3)_2$ or $MnCl_2$) (12.5 mM in degassed water) and H_2O_2 (4.17 mM in degassed water) dropwise to the reaction mixture at a rate of 31.3 μL/min using a pump under gentle stirring. Meanwhile maintain the pH of the reaction mixture at 8.5 with 50 mM NaOH by using a pH titrator.
▲ CRITICAL STEP The mineralization reaction produces H^+ ions. Herein, NaOH is used to maintain the reaction pH at 8.5. Low pH values will lower the mineralizing efficiency.
? TROUBLESHOOTING

9 After 10, 30 or 50 min of dropping, about 1,000, 3,000 and 5,000 atoms, respectively, per HFn nanocage should have dropped into the reaction solution. React for additional 5 min after the addition of all reagents.
▲ CRITICAL STEP The dropping time should not exceed 60 min (including the next step) to prevent HFn precipitation due to the overloading of metal cores.
10 Add 1 mL of 300 mM sodium citrate to chelate any free metal ions.
11 Open the glove box, take the reaction vial out and clean up the glove box.
12 Collect the mineralized HFn (HFn@Fe_3O_4, HFn@Co_3O_4 or HFn@MnO_2) by centrifugation at 12,000*g* for 15 min at 4 °C to remove precipitation, and transfer the supernatant to a clean tube.
13 Ultrafilter the collected products to replace the buffer with PBS buffer.
14 Quantify the concentration of HFn using a BCA protein assay kit.
▲ CRITICAL STEP The blown background of the mineralized HFn (M–HFn) usually interferes with the concentration measurement of M–HFn. The same concentration of M–HFn should thus be used as the blank control.
? TROUBLESHOOTING
15 Quantify the mineral content using inductively coupled plasma optical emission spectrometry (ICP-OES).
▲ CRITICAL STEP For details of how to quantify the mineral content using ICP-OES, please refer to the Supplementary Methods.
■ PAUSE POINT Keep M–HFn in PBS buffer. Filter-sterilize (0.22 μm), and store at 4 °C for a maximum of 6 months.

Procedure 2: encapsulation of doxorubicin within HFn nanocage ● Timing ~3 d

▲ CRITICAL This procedure produces ~80 mg HFn–Dox (with ~4.6 mg doxorubicin inside). The treatment dose we use for mice is ~10 mg/kg body weight (doxorubicin equivalents). The body weight of a mouse is ~25 g. Thus, this procedure produces sufficient HFn–Dox to treat ~18 mice at this scale.
1 Dilute HFn stock solution (10 mg/mL in 20 mM Tris-HCl, pH 8.0, containing 100 mM NaCl and 30% glycerin) in 100 mL urea solution (8 M) to a final concentration of 1 mg/mL, and gently stir for 30 min at RT to ensure complete dissociation.
2 Add doxorubicin stock solution to the reaction mixture to a final concentration of 0.2 mg/mL.
▲ CRITICAL STEP The doxorubicin solution should be handled in the dark to minimize photodegradation.
3 Incubate the mixture for 10 min in the dark with gentle stirring.
4 Transfer the mixture to a dialysis bag (MWCO: 14,000 Da), and dialyze against gradient concentrations of urea solution (7, 5, 3, 2, 1 and 0 M, each for 4 h) containing 1 mg/mL of doxorubicin at 4 °C to reassemble HFn nanocages gradually. The urea gradient dialysis will encapsulate the doxorubicin in the reaction mixture within HFn nanocages.
? TROUBLESHOOTING
5 Dialyze the resulting solution against PBS buffer overnight to remove the free doxorubicin.
6 Collect the final product in the tubes, and protect from light.
7 Quantify the concentration of HFn by using a BCA protein assay kit, and measure the absorbance at 485 nm to determine the quantity of the encapsulated doxorubicin.
8 Calculate the final molar ratio of doxorubicin to HFn nanocage by dividing the molar concentration of doxorubicin by the molar concentration of HFn.
■ PAUSE POINT As the prepared doxorubicin loaded HFn (HFn–Dox) is sensitive to light, the final product should be stored in the dark and in a freezer at 4 °C in PBS buffer for a maximum of 12 months after sterilization by 0.22 μm filtration. It is always preferable to divide the product into aliquots for storage to reduce the risk of decomposition resulting from multiple freeze–thaw cycles when product is removed.

Procedure 3: encapsulation of Gd^{3+} within the HFn nanocage ● Timing ~20 h

▲ CRITICAL The procedure produces ~45 mg of Gd^{3+}-encapsulated HFn–His protein (with ~4.32 μmol Gd^{3+} inside). We use a treatment dose for mice of 10 μmol/kg body weight (Gd^{3+} ion equivalents). The body weight of a mouse is ~25 g. Thus, following the procedure at this scale produces sufficient HFn–His–Gd^{3+} to treat ~17 mice.

1 Dilute the HFn–His stock solution (10 mg/mL in 20 mM Tris-HCl, pH 8.0, containing 100 mM NaCl and 30% glycerin) in 50 mL of 20 mM Tris-HCl (pH 8.0, 100 mM NaCl) buffer to a final concentration of 1 mg/mL. Incubate the mixture in a thermostatic 60 °C water bath for 30 min with gentle stirring.
2 Dilute the gadolinium ion stock solution in deionized water to a concentration of 400 μM.
3 Add the prepared gadolinium ion solution dropwise to the reaction mixture (being gently stirred in the thermostatic 60 °C water bath) at a rate of 100 μL/min using a pump for 100 min.
? TROUBLESHOOTING
4 Gently stir the reaction mixture in the thermostatic 60 °C water bath for an additional 140 min, during which time the gadolinium ions should go through the heat-enlarged hydrophilic channels and be chelated by the 8 × His peptides on the inner surface of HFn–His nanocage. Afterwards, take the reaction vial out of the thermostatic 60 °C water bath. After the reaction mixture cools down spontaneously to RT, the enlarged hydrophilic channels will return back to their natural compact status. Thus, the gadolinium ions will be encapsulated within the HFn–His nanocage.
5 Centrifuge the mixture at 12,000*g* for 30 min to remove the denatured proteins.
6 Place the supernatant in dialysis bag (MWCO: 14,000 Da), and dialyze it overnight against PBS buffer at 4 °C to remove free gadolinium ions.
7 Quantify the concentration of HFn–His using a BCA protein assay kit, and determine the encapsulated gadolinium using ICP-OES.
■ PAUSE POINT Dissolve the gadolinium-loaded HFn–His (HFn–His–Gd^{3+}) in PBS buffer. Filter-sterilize (0.22 μm), and store at 4 °C for a maximum of 6 months.

Procedure 4: encapsulation of $^{64}Cu^{2+}$ radioisotope within the HFn nanocage ● Timing ~3 h

▲ CRITICAL The procedure produces ~4.5 mg of $^{64}Cu^{2+}$-encapsulated HFn–His protein (with ~5 mCi of $^{64}Cu^{2+}$ ions inside). We use a treatment dose for each mouse of ~100 μCi ($^{64}Cu^{2+}$ ion equivalents). At this scale, this procedure makes sufficient $^{64}Cu^{2+}$-encapsulated HFn–His protein to treat ~50 mice.
1 Dissolve the HFn–His stock solution (10 mg/mL in 20 mM Tris-HCl, pH 8.0, containing 100 mM NaCl and 30% glycerin) in 5 mL of 20 mM Tris-HCl (pH 8.0, 100 mM NaCl) buffer to a final concentration of 1 mg/mL. Incubate the mixture in a thermostatic 60 °C water bath for 30 min with gentle shaking.
▲ CRITICAL STEP The optimized concentration for $^{64}Cu^{2+}$ encapsulation is 1 mg/mL HFn–His. Low concentrations of ferritin nanocage require large volumes when scaling up the manufacturing process. However, concentrations >1 mg mL^{-1} need longer incubations to get HFn–His saturated with $^{64}Cu^{2+}$. Because of the short half-life of $^{64}Cu^{2+}$ (12.7 h), it is important to reduce the total preparation time for successful application of $^{64}Cu^{2+}$-loaded ferritin.
2 While gently shaking, add ~30 mCi of $^{64}CuCl_2$ into the reaction vial.
! CAUTION Follow appropriate radiation safety measures for Steps 2–5.
▲ CRITICAL STEP This solution should be used only on the day of preparation.
? TROUBLESHOOTING
3 Incubate the mixture in a thermostatic water bath at a temperature of 60–65 °C for 1 h while gently shaking the reaction vial, and then cool to RT.
▲ CRITICAL STEP The temperature of the loading reaction should be in the range of 60–65 °C for optimal loading efficiency.
4 Purify the products on a PD-10 desalting column to remove free $^{64}Cu^{2+}$ using PBS buffer as eluent. Collect the fractions, measure the radioactivity in each fraction and combine the fractions containing the most radioactivity.
▲ CRITICAL STEP Because of the short half-life of $^{64}Cu^{2+}$ (12.7 h), we recommend using column filtration, which is faster than other methods such as dialysis, to purify the radio-loaded HFn–His.
? TROUBLESHOOTING
5 Determine the concentration of HFn–His using a BCA protein assay kit. Calculate the specific radioactivity as mCi $^{64}Cu^{2+}$ per mg HFn–His.
▲ CRITICAL STEP Because of the short half-life of $^{64}Cu^{2+}$ (12.7 h), it is important to reduce the number of preparation steps, the overall production and purification time for successful application of $^{64}Cu^{2+}$-loaded HFn–His in living systems.

Troubleshooting

Troubleshooting advice can be found in Table 3.

Table 3 | Troubleshooting table

Step	Problem	Possible reason	Solution
Reagent setup: preparation of HFn and HFn-His	Protein precipitation during purification	Local temperature is too high due to uneven heating during purification	Heat the supernatant that contains the target protein with continuous stirring
Reagent setup: preparation of HFn and HFn-His	Low protein yield	*Escherichia coli* cells are too old	Prepare fresh *Escherichia coli* cells
Procedure 1, Step 3	Oxygen concentration can not be maintained at <600 ppm	Glove box is not airtight	Find the leaks and repair them
Procedure 1, Step 8	Humidity too high in the glove box	Water evaporation due to the water bath	Put a layer of silicone oil on the water bath
Procedure 1, Step 14	The quantified concentration of M-HFn is incorrect	The blown background of M-HFn interferes with the concentration measurement	Use the same concentration of M-HFn as blank
Procedure 3, Step 3	Precipitation generation during experiment	Local concentration of gadolinium ions is too high	Gadolinium ion solution should be added slowly, and reaction mixture must be efficiently stirred upon addition of gadolinium ions
Procedure 4, Step 2	Protein precipitation during experiment	Local concentration of $^{64}CuCl_2$ is too high	$^{64}CuCl_2$ solution should be added slowly, and the reaction mixture must be efficiently shaken on addition of $^{64}CuCl_2$
Procedure 4, Step 4	Low radiochemical purity	Insufficient purification	Repeat PD-10 purification or, alternatively, apply ultrafiltration during the purification steps

Timing

Reagent setup, preparation of HFn and HFn–His nanocages: 2 d
Procedure 1, encapsulation of metal oxide NPs within HFn nanocages: 5 h
Procedure 2, doxorubicin loading within HFn nanocages: 3 d
Procedure 3, Gd^{3+} loading within HFn nanocages: 20 h
Procedure 4, $^{64}Cu^{2+}$ radio-loading within HFn nanocages: 3 h

Anticipated results

The preparation of HFn and HFn–His protein nanocages is straightforward if undertaken as described. SEC purification is required to achieve >90% protein purity (Fig. 4). Figure 4 shows typical SEC and electron cryo-microscopy (cryo-EM) images of purified HFn and HFn–His protein nanocages. Both the prepared HFn and HFn–His monodisperse in solution with well-defined spherical morphology (Fig. 4). HFn and HFn–His produced as described should be of sufficient quality for encapsulation and loading of various cargoes for most purposes.

HFn and HFn–His are stable enough to withstand heating at 70 °C for 15 min while being purified from *Escherichia coli*. Further evaluation of stability demonstrated that the obtained HFn and HFn–His nanocages are stable and do not dissociate over prolonged periods of at least 6 months at 4 °C or at −80 °C for up to 3 years in saline. In addition, the protein nanocages are also stable in serum at 37 °C with minor dissociation over 60 h of incubation, suggesting the ferritin nanocarriers will be sufficiently robust to retain their drug load during transit through the systemic circulation.

Figure 1 presents an example of results obtained from using this protocol to prepare Fe, Co and Mn oxide mineralized HFn NPs (M–HFn). The cryo-EM images clearly show the formation of uniformly spherical and monodispersed nanocores encapsulated within the HFn nanocages (Fig. 1b). Circular dichroism spectrum of M–HFn NPs is almost identical to that of HFn nanocages (Supplementary Fig. 1), indicating that the loading process does not substantially perturb the structural conformation of HFn nanocages and the encapsulated metal oxide core is sequestered within the protein nanocages. We recommend users also characterize M–HFn NPs using dynamic light

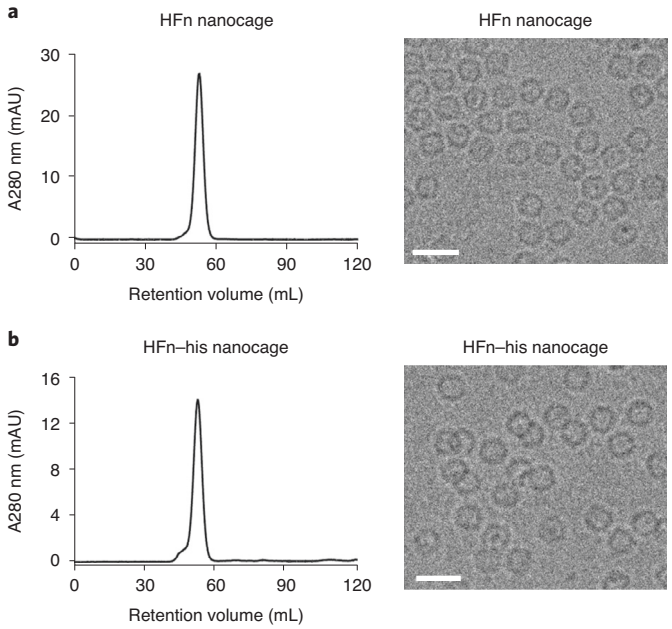

Fig. 4 | Characterization of HFn and HFn–His nanocages. a,**b**, Representative SEC analysis (left) and cryo-EM characterization (right) of HFn (**a**) and HFn–His nanocages (**b**). Scale bar, 20 nm. For details of how to perform SEC and cryo-EM characterization, please refer to the Supplementary Methods.

scattering (DLS), transmission electron microscopy and X-ray photoelectron spectroscopy to confirm the formation of metal nanocores within the cavity of each ferritin nanocage[40,45–50]. HFn encapsulated Fe_3O_4, Co_3O_4 and MnO_2 NPs can be successfully prepared using this protocol. However, whether this protocol can be used to encapsulate other metal oxide NPs within HFn requires further verification and investigation. To date, >50 types of NPs have been synthesized within the cavity of ferritin nanocage by modified versions of the described procedure, including TiO_2, Gd_2O_3, CeO_2, ZnSe, CdS, CdSe, Au, CuS, CuFe, CoPt, CoNi, Au-Ag and Ag NPs etc. (Table 1), suggesting that the ferritin vehicle system is universal and can be easily used.

Figure 2 shows a typical example of results obtained from the preparation of doxorubicin-loaded HFn nanocages (HFn–Dox). The loading of doxorubicin into HFn nanocages depends on electrostatic interactions as doxorubicin can easily bind to the negatively charged internal surface of ferritin in the neutral loading buffer[10,17]. The representative SEC results show the successful loading of doxorubicin into HFn nanocages (Fig. 2b). The amount of encapsulated doxorubicin can be determined by measuring the absorbance at 485 nm. Typical DLS results show that the prepared HFn–Dox has a narrow size distribution, and there is no substantial difference observed in size between HFn and HFn–Dox (Fig. 2c).

Figure 3 shows typical results following the use of this protocol to load Gd^{3+} or $^{64}Cu^{2+}$ within HFn–His nanocages. The representative energy-dispersive X-ray spectroscopy analysis shows the final product is composed of Gd element (Fig. 3b), indicating the successful loading of Gd^{3+} within HFn–His nanocages (HFn–His@Gd^{3+}). Figure 3c shows a typical size-exclusion HPLC radiochromatogram of $^{64}Cu^{2+}$-loaded HFn–His nanocages (HFn–His@$^{64}Cu^{2+}$). The retention times of the peaks in the UV trace and the radioactivity trace are identical, suggesting the successful loading of $^{64}Cu^{2+}$ within HFn–His nanocages. In this case, the radiochemical purity was >98% as determined by size-exclusion HPLC (Fig. 3c).

Table 4 presents the typical cargo loading efficiency into ferritin nanocages and cargo/protein recovery yield after loading using this protocol. In this particular analysis, the mineral content, including Fe, Co, Mn and Gd encapsulated into HFn nanocages was determined using ICP-OES (as described in the Supplementary Methods). The encapsulated doxorubicin was quantified by measuring the absorbance at 485 nm, and the HFn concentration was determined by using BCA protein assay kit. The radio-loading efficiency and radioactivity recovery were determined by measuring the specific radioactivity after purification. The cargo-loaded nanocages were stable in saline at 4 °C with minor cargo release over 6 months as determined by monitoring by size-exclusion HPLC. Furthermore, the cargo-loaded nanocages were also stable in 37 °C serum, with no substantial cargo release

Table 4 | Cargo loading efficiency and recovery following the use of this protocol

Ferritin	Cargo	Number of loaded cargos per ferritin	Protein recovery yield (%)	Cargo recovery yield (%)
HFn	Fe	3,186 ± 188	87 ± 9	64 ± 4
HFn	Co	2,814 ± 268	81 ± 12	56 ± 5
HFn	Mn	2,200 ± 342	73 ± 11	44 ± 7
HFn	Doxorubicin	53 ± 12	84 ± 6	35 ± 9
HFn-His	Gd^{3+}	48 ± 5	91 ± 6	13 ± 3
HFn-His	$^{64}Cu^{2+}$	1.1 ± 0.2 μCi/μg	90 ± 7	17 ± 4

Values indicate average ± SD. Underlying data are available in Supplementary Table 1.

or serum binding over a 48 h period of incubation, suggesting that the cargo-loaded nanocages will be sufficiently stable to retain their cargoes during transit through the systemic circulation.

Reporting Summary

Further information on research design is available in the Nature Research Reporting Summary linked to this article.

Data availability

Source data are provided with this paper.

References

1. Kim, B. Y. S., Rutka, J. T. & Chan, W. C. W. Nanomedicine. *N. Engl. J. Med.* **363**, 2434–2443 (2010).
2. Meel, R. et al. Smart cancer nanomedicine. *Nat. Nanotechnol.* **14**, 1007–1017 (2019).
3. Harmsen, S., Wall, M. A., Huang, R. & Kircher, M. F. Cancer imaging using surface-enhanced resonance Raman scattering nanoparticles. *Nat. Protoc.* **12**, 1400–1414 (2017).
4. Nam, J. et al. Cancer nanomedicine for combination cancer immunotherapy. *Nat Rev. Mater.* **4**, 398–414 (2019).
5. Sanhai, W. R., Sakamoto, J. H., Canady, R. & Ferrari, M. Seven challenges for nanomedicine. *Nat. Nanotechnol.* **3**, 242–244 (2008).
6. Shi, J., Kantoff, P. W., Wooster, R. & Farokhzad, O. C. Cancer nanomedicine: progress, challenges and opportunities. *Nat. Rev. Cancer* **17**, 20–37 (2017).
7. Docter, D. et al. Quantitative profiling of the protein coronas that form around nanoparticles. *Nat. Protoc.* **9**, 2030–2044 (2014).
8. Martin, J. D., Cabral, H., Stylianopoulos, T. & Jain, R. K. Improving cancer immunotherapy using nanomedicines: progress, opportunities and challenges. *Nat. Rev. Clin. Oncol.* **17**, 251–266 (2020).
9. Zhang, J. et al. Biochemistry of mammalian ferritins in the regulation of cellular iron homeostasis and oxidative responses. *Sci. China Life Sci.* **64**, 352–362 (2021).
10. Harrison, P. M. & Arosio, P. The ferritins: molecular properties, iron storage function and cellular regulation. *Biochim. Biophys. Acta* **1275**, 161–203 (1996).
11. Fan, K. et al. Magnetoferritin nanoparticles for targeting and visualizing tumour tissues. *Nat. Nanotechnol.* **7**, 459–464 (2012).
12. Li, L. et al. Binding and uptake of H-ferritin are mediated by human transferrin receptor-1. *Proc. Natl Acad. Sci. USA* **107**, 3505–3510 (2010).
13. Zhen, Z. et al. RGD-modified apoferritin nanoparticles for efficient drug delivery to tumors. *ACS Nano* **7**, 4830–4837 (2013).
14. Lin, X. et al. Hybrid ferritin nanoparticles as activatable probes for tumor imaging. *Angew. Chem. Int. Ed. Engl.* **50**, 1569–1572 (2011).
15. Jutz, G. N. et al. Ferritin: a versatile building block for bionanotechnology. *Chem. Rev.* **115**, 1653–1701 (2015).
16. Gao, F. et al. Hypoxia-tropic nanozymes as oxygen generators for tumor-favoring theranostics. *Biomaterials.* **230**, 119635 (2020).
17. Liang, M. et al. H-ferritin–nanocaged doxorubicin nanoparticles specifically target and kill tumors with a single-dose injection. *Proc. Natl Acad. Sci. USA* **111**, 14900–14905 (2014).
18. Wang, T. et al. Bioengineered magnetoferritin nanozymes for pathological identification of high-risk and ruptured atherosclerotic plaques in humans. *Nano Res.* **12**, 863–868 (2019).
19. Zhao, Y. et al. Bioengineered magnetoferritin nanoprobes for single-dose nuclear-magnetic resonance tumor imaging. *ACS Nano* **10**, 4184–4191 (2016).

20. Li, Y. et al. Nanoparticle ferritin-bound erastin and rapamycin: a nanodrug combining autophagy and ferroptosis for anticancer therapy. *Biomater. Sci.* **7**, 3779–3787 (2019).
21. Cheng, X. et al. TfR1 binding with H-ferritin nanocarrier achieves prognostic diagnosis and enhances the therapeutic efficacy in clinical gastric cancer. *Cell Death Dis.* **11**, 1–13 (2020).
22. Macone, A. et al. Ferritin nanovehicle for targeted delivery of cytochrome C to cancer cells. *Sci. Rep.* **9**, 11749 (2019).
23. Zhang, C., Zhang, X. & Zhao, G. Ferritin nanocage: a versatile nanocarrier utilized in the field of food, nutrition, and medicine. *Nanomaterials (Basel)* **10**, 1894 (2020).
24. Tetter, S. & Hilvert, D. Enzyme encapsulation by a ferritin cage. *Angew. Chem. Int. Ed. Engl.* **56**, 14933–14936 (2017).
25. Khoshnejad, M., Parhiz, H., Shuvaev, V. V., Dmochowski, I. J. & Muzykantov, V. R. Ferritin-based drug delivery systems: hybrid nanocarriers for vascular immunotargeting. *J. Control. Release* **282**, 13–24 (2018).
26. Li, L. et al. Ferritin-mediated siRNA delivery and gene silencing in human tumor and primary cells. *Biomaterials* **98**, 143–151 (2016).
27. Wang, Z. et al. Metal ion assisted interface re-engineering of a ferritin nanocage for enhanced biofunctions and cancer therapy. *Nanoscale* **10**, 1135–1144 (2018).
28. Uchida, M. et al. Targeting of cancer cells with ferrimagnetic ferritin cage nanoparticles. *J. Am. Chem. Soc.* **128**, 16626–16633 (2006).
29. Truffi, M. et al. Ferritin nanocages: a biological platform for drug delivery, imaging and theranostics in cancer. *Pharmacol. Res.* **107**, 57–65 (2016).
30. Wang, Z. et al. Functional ferritin nanoparticles for biomedical applications. *Front. Chem. Sci. Eng.* **11**, 633–646 (2017).
31. Wang, Z. et al. Biomineralization-inspired synthesis of copper sulfide–ferritin nanocages as cancer theranostics. *ACS Nano* **10**, 3453–3460 (2016).
32. Lin, X. et al. Chimeric ferritin nanocages for multiple function loading and multimodal imaging. *Nano Lett.* **11**, 814–819 (2011).
33. Chauhan, V. P. et al. Normalization of tumour blood vessels improves the delivery of nanomedicines in a size-dependent manner. *Nat. Nanotechnol.* **7**, 383–388 (2012).
34. Huang, X. et al. Protein nanocages that penetrate airway mucus and tumor tissue. *Proc. Natl Acad. Sci. USA* **114**, E6595–E6602 (2017).
35. Li, X. et al. Epidermal growth factor–ferritin H-chain protein nanoparticles for tumor active targeting. *Small* **8**, 2505–2514 (2012).
36. Bitonto, V. et al. L-ferritin: a theranostic agent of natural origin for MRI visualization and treatment of breast cancer. *J. Control. Release* **319**, 300–310 (2020).
37. Zhen, Z. et al. Ferritin nanocages to encapsulate and deliver photosensitizers for efficient photodynamic therapy against cancer. *ACS Nano* **7**, 6988–6996 (2013).
38. Kuruppu, A. I. et al. An apoferritin-based drug delivery system for the tyrosine kinase inhibitor gefitinib. *Adv. Healthc. Mater.* **4**, 2816–2821 (2015).
39. Zhou, H. et al. Mn-loaded apolactoferrin dots for in vivo MRI and NIR-II cancer imaging. *J. Mater. Chem. C* **7**, 9448–9454 (2019).
40. Fan, J. et al. Direct evidence for catalase and peroxidase activities of ferritin–platinum nanoparticles. *Biomaterials* **32**, 1611–1618 (2011).
41. Yang, Z. et al. Encapsulation of platinum anticancer drugs by apoferritin. *Chem. Commun. (Camb)* **33**, 3453–3455 (2007).
42. Kim, M. et al. pH-dependent structures of ferritin and apoferritin in solution: disassembly and reassembly. *Biomacromolecules* **12**, 1629–1640 (2011).
43. He, J., Fan, K. & Yan, X. Ferritin drug carrier (FDC) for tumor targeting therapy. *J. Control Release* **311**, 288–300 (2019).
44. Tesarova, B., Musilek, K., Rex, S. & Heger, Z. Taking advantage of cellular uptake of ferritin nanocages for targeted drug delivery. *J. Control Release* **325**, 176–190 (2020).
45. Liu, X. et al. Apoferritin–CeO 2 nano-truffle that has excellent artificial redox enzyme activity. *Chem. Commun. (Camb)* **48**, 3155–3157 (2012).
46. Iwahori, K., Yoshizawa, K., Muraoka, M. & Yamashita, I. Fabrication of ZnSe nanoparticles in the apoferritin cavity by designing a slow chemical reaction system. *Inorg. Chem.* **44**, 6393–6400 (2005).
47. Naito, M., Iwahori, K., Miura, A., Yamane, M. & Yamashita, I. Circularly polarized luminescent CdS quantum dots prepared in a protein nanocage. *Angew. Chem. Int. Ed. Engl.* **49**, 7006–7009 (2010).
48. Yamashita, I., Hayashi, J. & Hara, M. Bio-template synthesis of uniform CdSe nanoparticles using cage-shaped protein, apoferritin. *Chem. Lett.* **33**, 1158–1159 (2004).
49. Klem, M. T., Mosolf, J., Young, M. & Douglas, T. Photochemical mineralization of europium, titanium, and iron oxyhydroxide nanoparticles in the ferritin protein cage. *Inorg. Chem.* **47**, 2237–2239 (2008).
50. Hosein, H.-A., Strongin, D. R., Allen, M. & Douglas, T. Iron and cobalt oxide and metallic nanoparticles prepared from ferritin. *Langmuir.* **20**, 10283–10287 (2004).
51. Monti, D. M., Ferraro, G. & Merlino, A. Ferritin-based anticancer metallodrug delivery: crystallographic, analytical and cytotoxicity studies. *Nanomedicine* **20**, 101997 (2019).
52. Falvo, E. et al. Antibody–drug conjugates: targeting melanoma with cisplatin encapsulated in protein-cage nanoparticles based on human ferritin. *Nanoscale* **5**, 12278–12285 (2013).

53. Liu, W. et al. Target delivering paclitaxel by ferritin heavy chain nanocages for glioma treatment. *J. Control. Release* **323**, 191–202 (2020).
54. Liu, M., Zhu, Y., Wu, T., Cheng, J. & Liu, Y. Nanobody-ferritin conjugate for targeted photodynamic therapy. *Chemistry* **26**, 7442–7450 (2020).
55. Lee, E. J. et al. Engineered proteinticles for targeted delivery of siRNA to cancer cells. *Adv. Funct. Mater.* **25**, 1279–1286 (2015).
56. Wang, W. et al. Ferritin nanoparticle-based SpyTag/SpyCatcher-enabled click vaccine for tumor immunotherapy. *Nanomedicine* **16**, 69–78 (2019).
57. Falvo, E. et al. The presence of glutamate residues on the PAS sequence of the stimuli-sensitive nano-ferritin improves in vivo biodistribution and mitoxantrone encapsulation homogeneity. *J. Control. Release* **275**, 177–185 (2018).
58. Huang, P. et al. Dye-loaded ferritin nanocages for multimodal imaging and photothermal therapy. *Adv. Mater.* **26**, 6401–6408 (2014).
59. Chen, L. et al. Encapsulation of β-carotene within ferritin nanocages greatly increases its water-solubility and thermal stability. *Food Chem.* **149**, 307–312 (2014).
60. Huang, C. et al. Ultra-high loading of sinoporphyrin sodium in ferritin for single-wave motivated photothermal and photodynamic co-therapy. *Biomater. Sci.* **5**, 1512–1516 (2017).
61. Li, K. et al. Multifunctional ferritin cage nanostructures for fluorescence and MR imaging of tumor cells. *Nanoscale* **4**, 188–193 (2012).
62. Kim, H.-K. et al. Highly brain-permeable apoferritin nanocage with high dysprosium loading capacity as a new T2 contrast agent for ultra-high field magnetic resonance imaging. *Biomaterials* **243**, 119939 (2020).
63. Crich, S. G. et al. Magnetic resonance visualization of tumor angiogenesis by targeting neural cell adhesion molecules with the highly sensitive gadolinium-loaded apoferritin probe. *Cancer Res.* **66**, 9196–9201 (2006).
64. Cai, Y., Wang, Y., Zhang, T. & Pan, Y. Gadolinium-labeled ferritin nanoparticles as T 1 contrast agents for magnetic resonance imaging of tumors. *ACS Appl. Nano Mater.* **3**, 8771–8783 (2020).
65. Sánchez, P. et al. MRI relaxation properties of water-soluble apoferritin-encapsulated gadolinium oxide-hydroxide nanoparticles. *Dalton Trans.* **5**, 800–804 (2009).
66. Liang, M. et al. Bioengineered H-ferritin nanocages for quantitative imaging of vulnerable plaques in atherosclerosis. *ACS Nano* **12**, 9300–9308 (2018).
67. Jiang, B. et al. Biomineralization synthesis of the cobalt nanozyme in SP94-ferritin nanocages for prognostic diagnosis of hepatocellular carcinoma. *ACS Appl. Mater. Interfaces* **11**, 9747–9755 (2019).
68. Butts, C. A. et al. Directing noble metal ion chemistry within a designed ferritin protein. *Biochemistry* **47**, 12729–12739 (2008).
69. Iwahori, K., Takagi, R., Kishimoto, N. & Yamashita, I. A size controlled synthesis of CuS nano-particles in the protein cage, apoferritin. *Mater. Lett.* **65**, 3245–3247 (2011).
70. Gálvez, N., Sánchez, P. & Domínguez-Vera, J. M. Preparation of Cu and CuFe Prussian Blue derivative nanoparticles using the apoferritin cavity as nanoreactor. *Dalton Trans.* **15**, 2492–2494 (2005).
71. Gálvez, N. et al. Apoferritin-encapsulated Ni and Co superparamagnetic nanoparticles. *J. Mater. Chem.* **16**, 2757–2761 (2006).
72. Kashanian, S., Tarighat, F. & Rafipour, R. Biomimetic synthesis of cobalt nanoparticle using apoferritin and its application in electrochemical reaction to detect glucose. *New Biotechnol.* **25**, S376 (2009).
73. Kashanian, S., Tarighat, F. A., Rafipour, R. & Abbasi-Tarighat, M. Biomimetic synthesis and characterization of cobalt nanoparticles using apoferritin, and investigation of direct electron transfer of Co (NPs)–ferritin at modified glassy carbon electrode to design a novel nanobiosensor. *Mol. Biol. Rep.* **39**, 8793–8802 (2012).
74. Warne, B., Kasyutich, O. I., Mayes, E. L., Wiggins, J. A. L. & Wong, K. K. W. Self assembled nanoparticulate Co: Pt for data storage applications. *IEEE Trans. Magn.* **36**, 3009–3011 (2000).
75. Gálvez, N. et al. A bioinspired approach to the synthesis of bimetallic CoNi nanoparticles. *Inorg. Chem.* **49**, 1705–1711 (2010).
76. Okuda, M., Iwahori, K., Yamashita, I. & Yoshimura, H. Fabrication of nickel and chromium nanoparticles using the protein cage of apoferritin. *Biotechnol. Bioeng.* **84**, 187–194 (2003).
77. Polanams, J., Ray, A. D. & Watt, R. K. Nanophase iron phosphate, iron arsenate, iron vanadate, and iron molybdate minerals synthesized within the protein cage of ferritin. *Inorg. Chem.* **44**, 3203–3209 (2005).
78. Shin, Y., Dohnalkova, A. & Lin, Y. Preparation of homogeneous gold–silver alloy nanoparticles using the apoferritin cavity as a nanoreactor. *J. Phys. Chem. C* **114**, 5985–5989 (2010).
79. Provaznik, I., Vrba, R. & Kizek, R. Electrochemical behaviour of apoferritin encapsulating of silver (I) ions and its application for treatment of *Staphylococcus aureus*. *Int. J. Electrochem. Sci.* **7**, 6378–6395 (2012).
80. Sennuga, A., van Marwijk, J. & Whiteley, C. G. Multiple fold increase in activity of ferroxidase–apoferritin complex by silver and gold nanoparticles. *Nanomedicine* **9**, 185–193 (2013).
81. Turyanska, L. et al. The biocompatibility of apoferritin-encapsulated PbS quantum dots. *Small* **5**, 1738–1741 (2009).
82. Turyanska, L. et al. The differential effect of apoferritin-PbS nanocomposites on cell cycle progression in normal and cancerous cells. *J. Mater. Chem.* **22**, 660–665 (2012).
83. Hennequin, B. et al. Aqueous near-infrared fluorescent composites based on apoferritin-encapsulated PbS quantum dots. *Adv. Mater.* **20**, 3592–3596 (2008).
84. Du, D. et al. Nanoparticle-based immunosensor with apoferritin templated metallic phosphate label for quantification of phosphorylated acetylcholinesterase. *Biosens. Bioelectron.* **26**, 3857–3863 (2011).

85. Wu, H. et al. Apoferritin-templated yttrium phosphate nanoparticle conjugates for radioimmunotherapy of cancers. *J. Nanosci. Nanotechnol.* **8**, 2316–2322 (2008).
86. Wu, H., Engelhard, M. H., Wang, J., Fisher, D. R. & Lin, Y. Synthesis of lutetium phosphate–apoferritin core–shell nanoparticles for potential applications in radioimmunoimaging and radioimmunotherapy of cancers. *J. Mater. Chem.* **18**, 1779–1783 (2008).
87. Li, M., Viravaidya, C. & Mann, S. J. S. Polymer-mediated synthesis of ferritin-encapsulated inorganic nanoparticles. *Small* **3**, 1477–1481 (2007).
88. Zhang, W. et al. Prussian blue modified ferritin as peroxidase mimetics and its applications in biological detection. *J. Nanosci. Nanotechnol.* **13**, 60–67 (2013).
89. Hainfeld, J. F. Uranium-loaded apoferritin with antibodies attached: molecular design for uranium neutron-capture therapy. *Proc. Natl Acad. Sci. USA* **89**, 11064–11068 (1992).
90. Xing, R. et al. Characterization and cellular uptake of platinum anticancer drugs encapsulated in apoferritin. *J. Inorg. Biochem.* **103**, 1039–1044 (2009).
91. Zhang, Q. et al. Inlaying radiosensitizer onto the polypeptide shell of drug-loaded ferritin for imaging and combinational chemo-radiotherapy. *Theranostics* **9**, 2779–2790 (2019).
92. Kilic, M. A., Ozlu, E. & Calis, S. A novel protein-based anticancer drug encapsulating nanosphere: apoferritin-doxorubicin complex. *J. Biomed. Nanotechnol.* **8**, 508–514 (2012).
93. Cutrin, J. C., Crich, S. G., Burghelea, D., Dastru, W. & Aime, S. Curcumin/Gd loaded apoferritin: a novel "theranostic" agent to prevent hepatocellular damage in toxic induced acute hepatitis. *Mol. Pharm.* **10**, 2079–2085 (2013).
94. Lei, Y. et al. Targeted tumor delivery and controlled release of neuronal drugs with ferritin nanoparticles to regulate pancreatic cancer progression. *J. Control. Release* **232**, 131–142 (2016).

Acknowledgements

This work was supported by the following grants: National Key R&D Program of China (2017YFA0205501), National Natural Science Foundation of China (81722024 and 81571728), Youth Innovation Promotion (2014078 and Y201819) and Shenzhen Key Technologies R&D general program (Shenzhen Science & Technology Innovation, 2020, NO. 194).

Author contributions

All authors contributed to developing this protocol and writing this paper. M.L. supervised the project.

Competing interests

The authors declare no competing interests.

Additional information

Supplementary information The online version contains supplementary material available at https://doi.org/10.1038/s41596-021-00602-5.

Correspondence and requests for materials should be addressed to Minmin Liang.

Peer review information *Nature Protocols* thanks Pierpaolo Ceci, Insan Kim, Ichiro Yamashita and the other, anonymous reviewer(s) for their contribution to the peer review of this work.

Reprints and permissions information is available at www.nature.com/reprints.

Publisher's note Springer Nature remains neutral with regard to jurisdictional claims in published maps and institutional affiliations.

Received: 3 October 2020; Accepted: 5 July 2021;
Published online: 08 September 2021

Related links

Key references using this protocol

Fan, K. et al. *Nat. Nanotechnol.* **7**, 459–464 (2012): https://doi.org/10.1038/nnano.2012.90
Liang, M. et al. *Proc. Natl Acad. Sci.* **111**, 14900–14905 (2014): https://doi.org/10.1073/pnas.1407808111
Zhao, Y. et al. *ACS Nano*, **10**, 4184–4191(2016): https://doi.org/10.1021/acsnano.5b07408
Liang, M. et al. *ACS Nano* **12**, 9300–9308 (2018): https://doi.org/10.1021/acsnano.8b04158

nature research

Corresponding author(s): Minmin Liang

Last updated by author(s): May 20, 2021

Reporting Summary

Nature Research wishes to improve the reproducibility of the work that we publish. This form provides structure for consistency and transparency in reporting. For further information on Nature Research policies, see our Editorial Policies and the Editorial Policy Checklist.

Statistics

For all statistical analyses, confirm that the following items are present in the figure legend, table legend, main text, or Methods section.

n/a	Confirmed	
☐	☒	The exact sample size (*n*) for each experimental group/condition, given as a discrete number and unit of measurement
☐	☒	A statement on whether measurements were taken from distinct samples or whether the same sample was measured repeatedly
☒	☐	The statistical test(s) used AND whether they are one- or two-sided *Only common tests should be described solely by name; describe more complex techniques in the Methods section.*
☒	☐	A description of all covariates tested
☒	☐	A description of any assumptions or corrections, such as tests of normality and adjustment for multiple comparisons
☒	☐	A full description of the statistical parameters including central tendency (e.g. means) or other basic estimates (e.g. regression coefficient) AND variation (e.g. standard deviation) or associated estimates of uncertainty (e.g. confidence intervals)
☒	☐	For null hypothesis testing, the test statistic (e.g. *F*, *t*, *r*) with confidence intervals, effect sizes, degrees of freedom and *P* value noted *Give P values as exact values whenever suitable.*
☒	☐	For Bayesian analysis, information on the choice of priors and Markov chain Monte Carlo settings
☒	☐	For hierarchical and complex designs, identification of the appropriate level for tests and full reporting of outcomes
☒	☐	Estimates of effect sizes (e.g. Cohen's *d*, Pearson's *r*), indicating how they were calculated

Our web collection on statistics for biologists contains articles on many of the points above.

Software and code

Policy information about availability of computer code

Data collection	UNICORN 7, Digital Micrograph 3.9, DYNAMICS 7, Chirasean, Qtegra ISDS
Data analysis	Excel, GraphPad Prism

For manuscripts utilizing custom algorithms or software that are central to the research but not yet described in published literature, software must be made available to editors and reviewers. We strongly encourage code deposition in a community repository (e.g. GitHub). See the Nature Research guidelines for submitting code & software for further information.

Data

Policy information about availability of data

All manuscripts must include a data availability statement. This statement should provide the following information, where applicable:

- Accession codes, unique identifiers, or web links for publicly available datasets
- A list of figures that have associated raw data
- A description of any restrictions on data availability

We have provided a full data availability statement in the manuscript.

Field-specific reporting

Please select the one below that is the best fit for your research. If you are not sure, read the appropriate sections before making your selection.

☒ Life sciences ☐ Behavioural & social sciences ☐ Ecological, evolutionary & environmental sciences

For a reference copy of the document with all sections, see nature.com/documents/nr-reporting-summary-flat.pdf

Life sciences study design

All studies must disclose on these points even when the disclosure is negative.

Sample size	No biological or clinical samples used.
Data exclusions	No data is excluded.
Replication	No replication.
Randomization	No randomization.
Blinding	No blinding.

Reporting for specific materials, systems and methods

We require information from authors about some types of materials, experimental systems and methods used in many studies. Here, indicate whether each material, system or method listed is relevant to your study. If you are not sure if a list item applies to your research, read the appropriate section before selecting a response.

Materials & experimental systems

n/a	Involved in the study
☒	☐ Antibodies
☒	☐ Eukaryotic cell lines
☒	☐ Palaeontology and archaeology
☒	☐ Animals and other organisms
☒	☐ Human research participants
☒	☐ Clinical data
☒	☐ Dual use research of concern

Methods

n/a	Involved in the study
☒	☐ ChIP-seq
☒	☐ Flow cytometry
☒	☐ MRI-based neuroimaging